Arabidopsis CTP:phosphocholine cytidylyltransferase 1 is phosphorylated and inhibited by sucrose nonfermenting 1–related protein kinase 1 (SnRK1)

Received for publication, February 15, 2019, and in revised form, August 19, 2019 Published, Papers in Press, August 22, 2019, DOI 10.1074/jbc.RA119.008047

Kristian Mark P. Caldo[‡1], **Yang Xu**[‡1], **Lucas Falarz**[‡1], **Kethmi Jayawardhane**[‡], **Jeella Z. Acedo**[§], and **Guanqun Chen**[‡2]

From the Departments of [‡]*Agricultural, Food, and Nutritional Science and* [§]*Chemistry,University of Alberta, Edmonton, Alberta T6G 2G2, Canada*

Edited by Joseph M. Jez

De novo **phosphatidylcholine (PC) biosynthesis via the Kennedy pathway involves highly endergonic biochemical reactions that must be fine-tuned with energy homeostasis. Previous studies have shown that CTP:phosphocholine cytidylyltransferase (CCT) is an important regulatory enzyme in this pathway and that its activity can be controlled at both transcriptional and posttranslational levels. Here we identified an important additional mechanism regulating plant CCT1 activity. Comparative analysis revealed that *Arabidopsis* CCT1 (AtCCT1) contains catalytic and membrane-binding domains that are homologous to those of rat CCT1. In contrast, the C-terminal phosphorylation domain important for stringent regulation of rat CCT1 was apparently missing in AtCCT1. Instead, we found that AtCCT1 contains a putative consensus site (Ser-187) for modification by sucrose nonfermenting 1–related protein kinase 1 (SnRK1 or KIN10/SnRK1.1), involved in energy homeostasis. Phos-tag SDS-PAGE coupled with MS analysis disclosed that SnRK1 indeed phosphorylates AtCCT1 at Ser-187, and we found that AtCCT1 phosphorylation substantially reduces its activity by as much as 70%. An S187A variant exhibited decreased activity, indicating the importance of Ser-187 in catalysis, and this variant was less susceptible to SnRK1-mediated inhibition. Protein truncation and liposome binding studies indicated that SnRK1-mediated AtCCT1 phosphorylation directly affects the catalytic domain rather than interfering with phosphatidate-mediated AtCCT1 activation. Overexpression of the AtCCT1 catalytic domain in *Nicotiana benthamiana* leaves increased PC content, and SnRK1 co-expression reduced this effect. Taken together, our results suggest that SnRK1 mediates the phosphorylation and concomitant inhibition of AtCCT1, revealing an additional mode of regulation for this key enzyme in plant PC biosynthesis.**

Phosphatidylcholine (PC)[3] is the major membrane lipid constituent of most plant and animal cells. It also serves as substrate for fatty acyl desaturation, triacylglycerol (TAG) biosynthesis, oil body formation, as well as production of secondary messengers such as diacylglycerol (DAG) and phosphatidic acid (PA) (1, 2). *De novo* biosynthesis of PC through the CDP-choline pathway was first elucidated by Kennedy (3). In this pathway, choline is firstly phosphorylated by choline kinase in an ATP-dependent manner to produce phosphocholine. CTP: phosphocholine cytidylyltransferase (CCT) then transfers a cytidyl moiety from CTP to phosphocholine to yield CDP-choline. CDP-choline is then used by choline phosphotransferase as a phosphocholine donor to convert DAG to PC. This pathway provides the major amount of PC in plant cells, although small amounts can also be derived from phosphatidylethanolamine and phosphatidylserine (4, 5).

A number of studies have shown that, among the enzymes for *de novo* PC biosynthesis in plants, CCT catalyzes a key regulatory step (6, 7), and its activity is controlled at the transcriptional (7) and posttranslational levels (6). *Arabidopsis thaliana* (hereafter called *Arabidopsis*) *CCT* cDNAs were first identified through complementation of yeast deficient in corresponding *CCT* genes (8). *Arabidopsis* CCT1 (AtCCT1) was shown to be activated in the presence of increasing levels of PA upon inactivation of PA hydrolase (6). In addition, the PA-mediated activation of CCT in *Arabidopsis* was implicated in the proliferation of endoplasmic reticulum membranes, highlighting the important role of CCT as a key metabolic sensor in modulating membrane lipid homeostasis (6). Furthermore, overexpression of the cDNA encoding a constitutively active form of AtCCT1 led to increased fatty acid and PC content (6). Considering the importance of PC biosynthesis in cellular function, this process must be finely adjusted to the needs of the cells during various stages of plant growth and development as well as to the availability of substrates and the energy state of organisms.

This work was supported by University of Alberta start-up research grant RES0036786, Alberta Innovates grant AgFC2019F111R, Alberta Agriculture and Forestry grant AgFC2019F135R, Natural Sciences and Engineering Research Council of Canada discovery grant RGPIN-2016-05926, and Canada Research Chairs program grant RES0037649. The authors declare that they have no conflicts of interest with the contents of this article. The content is solely the responsibility of the authors and does not necessarily represent the official views of the National Institutes of Health.

This article contains Figs. S1–S6, Table S1, and supplemental Methods.

[1] These authors contributed equally to this work.

[2] To whom correspondence should be addressed: Tel.: 780-492-3148; E-mail: gc24@ualberta.ca.

[3] The abbreviations used are: PC, phosphatidylcholine; TAG, triacylglycerol; DAG, diacylglycerol; PA, phosphatidic acid; CCT, CTP:phosphocholine cytidylyltransferase; cDNA, complementary DNA; CD, catalytic domain; HMG-CoA, 3-hydroxy-3-methylglutaryl–CoA; Ni-NTA, nickel-nitrilotriacetic acid; TBS, Tris-buffered saline; DGAT1, diacylglycerol acyltransferase 1; WRI1, WRINKLED1.

Plant sucrose nonfermenting 1–related protein kinase 1 (SnRK1) is a serine/threonine kinase that acts as an energy sensor regulating cellular metabolism in response to stress, starvation, and various growth conditions (9). SnRK1 regulates the activity of key enzymes involved in various biosynthetic pathways of important cellular compounds, such as carbohydrates, amino acids, isoprenoids, and signaling sugars (10). As for carbohydrates, SnRK1 regulates two key enzymes, sucrose phosphate synthase and ADP-glucose pyrophosphorylase, in the biosynthesis of sucrose and starch, respectively (11, 12). This kinase also appears to modulate the transcription of carbohydrate metabolic genes, although the exact mechanisms have not yet been fully elucidated (13, 14).

SnRK1 also regulates storage lipid biosynthesis (15, 16). At the transcriptional level, SnRK1 regulates storage lipid metabolism by phosphorylating WRINKLED1 (WRI1), an important transcription factor controlling the expression of enzymes in late glycolysis and fatty acid biosynthesis (15, 16). At the post-translational level, our recent study found that SnRK1 regulates TAG accumulation through phosphorylation of diacylglycerol acyltransferase 1 (DGAT1), an enzyme catalyzing the final committed step in acyl-CoA– dependent TAG biosynthesis (17, 18). It was further noted that plant DGAT1 and CCT1 appear to share a common theme of regulation (19), with both having disordered regulatory domains and being activated by PA.

Considering that SnRK1 regulates storage lipid biosynthesis as well as a few other important pathways related to homeostasis in plant cells, it is interesting to explore whether SnRK1 also regulates membrane lipid biosynthesis. Furthermore, because DGAT1 is regulated by SnRK1 and shares a common theme of regulation with CCT, it would also be interesting to identify whether SnRK1 regulates CCT activity as well. In this study, sequence analysis identified that AtCCT1 has a putative SnRK1 phosphorylation site that is conserved among various plant species. Homology modeling with rat (*Rattus norvegicus*) CCT1 predicted that the putative phosphorylation site is localized in an accessible loop region. Incubation of recombinant AtCCT1 with SnRK1.1 (hereafter referred to as SnRK1) and subsequent LC-MS/MS analysis confirmed that SnRK1 phosphorylates AtCCT1 mainly at Ser-187, which is within the catalytic domain. The phosphorylated AtCCT1 displayed a substantial decrease in enzyme activity. Mutation of Ser-187 to alanine decreased the activity, and the S187A variant was less susceptible to inhibition by SnRK1. Further truncation mutagenesis showed that phosphorylation at this site affects the catalytic domain directly, leading to enzyme inhibition rather than interfering with PA-mediated activation. Transient expression of cDNA encoding the catalytic domain of AtCCT1 in *Nicotiana benthamiana* drove the accumulation of PC to higher levels than the control, whereas co-expression of the *AtCCT1* catalytic domain with *SnRK1* reduced the observed increase in PC content. These results indicated that SnRK1 regulates plant CCT1 via phosphorylation at Ser-187, which provides a mechanistic link between *de novo* PC biosynthesis and energy homeostasis.

Results

Arabidopsis CCT1 exhibits similar core functional domains as animal CCT1

Rat CCT1 has four functional domains that include the N-terminal signal for nuclear transport, catalytic core, membrane-binding regulatory domain, and C-terminal phosphorylation module (20, 21). To examine whether plant CCT1 has a similar structure as its animal homolog, the sequence of AtCCT1 was aligned with rat CCT1. As shown in Fig. 1*A* and Fig. S1, both CCT1s have homologous internal domains, whereas the terminal domains are highly divergent. The internal domains include the catalytic (Fig. 1*A*, *green*) and membrane-binding domains (Fig. 1*A*, *yellow*), which exhibit 59.3% and 24.2% sequence identities, respectively, between *Arabidopsis* and rat CCT1.

The catalytic domain of rat CCT1 is active in the absence of the membrane-binding and C-terminal domains (20). To probe whether *Arabidopsis* CCT1 has the same property, the cDNAs encoding AtCCT1, AtCCT1 catalytic domain ($AtCCT1_{1-197}$, hereafter referred to as AtCCT1-CD), and $AtCCT1_{1-221}$ were recombinantly expressed in *Escherichia coli* and partially purified through Ni-NTA (Fig. S2). $AtCCT1_{1-221}$ is included to check whether the catalytic domain in AtCCT1 extends beyond the last residue that aligned with the rat CCT catalytic domain. The activity of CCT1 was determined using a previously reported HPLC-based assay involving nonradiolabeled CTP and phosphocholine as substrates (22). CDP-choline was separated on a C18 column, and its amount was quantified based on the absorbance of the cytosine ring at 254 nm (Fig. S3). Similar to rat CCT1, purified AtCCT1-CD shows detectable CCT activity (Fig. 1*B*), indicating that the membrane-binding and C-terminal domains are not essential for catalysis.

Although the membrane-binding domain is not important for activity, it mediates lipid-dependent activation and autoinhibition in rat CCT1 (20). Because PA was identified previously as an activator of AtCCT1 in both *in vivo* and *in vitro* experiments (6), purified AtCCT1 and AtCCT1-CD were assayed under increasing concentrations of PA (Fig. 1*B*). The activity of AtCCT1 increased by 67-fold upon addition of 50 μM PA:50 μM PC vesicles. AtCCT1-CD, on the other hand, was constitutively active and was no longer activated by PA. Furthermore, AtCCT1 exhibited activities of 183 nmol CDP-choline min^{-1} mg $protein^{-1}$ when no lipid was added (Fig. 1*B*). Under the same condition, AtCCT1-CD and $AtCCT1_{1-221}$ were about 9-fold more active than AtCCT1, suggesting that the truncated region inhibits the enzyme. Altogether, these results show that the membrane-binding domain plays an important role in mediating both lipid-dependent activation and autoinhibition, which agrees with previous results on mammalian CCTs (23, 24). The rat CCT membrane-binding domain has different segments, such as the polybasic region, nonconserved portion, and autoinhibitory motif (25), that have been found to form amphipathic helices upon interaction with the membranes. In AtCCT1, the helical diagram of corresponding regions suggested a similar amphipathic property (Fig. 1*C*). The first two segments covering residues 197–230 can form α-helices, with a hydrophobic face composed of leucine, isoleucine, and valine

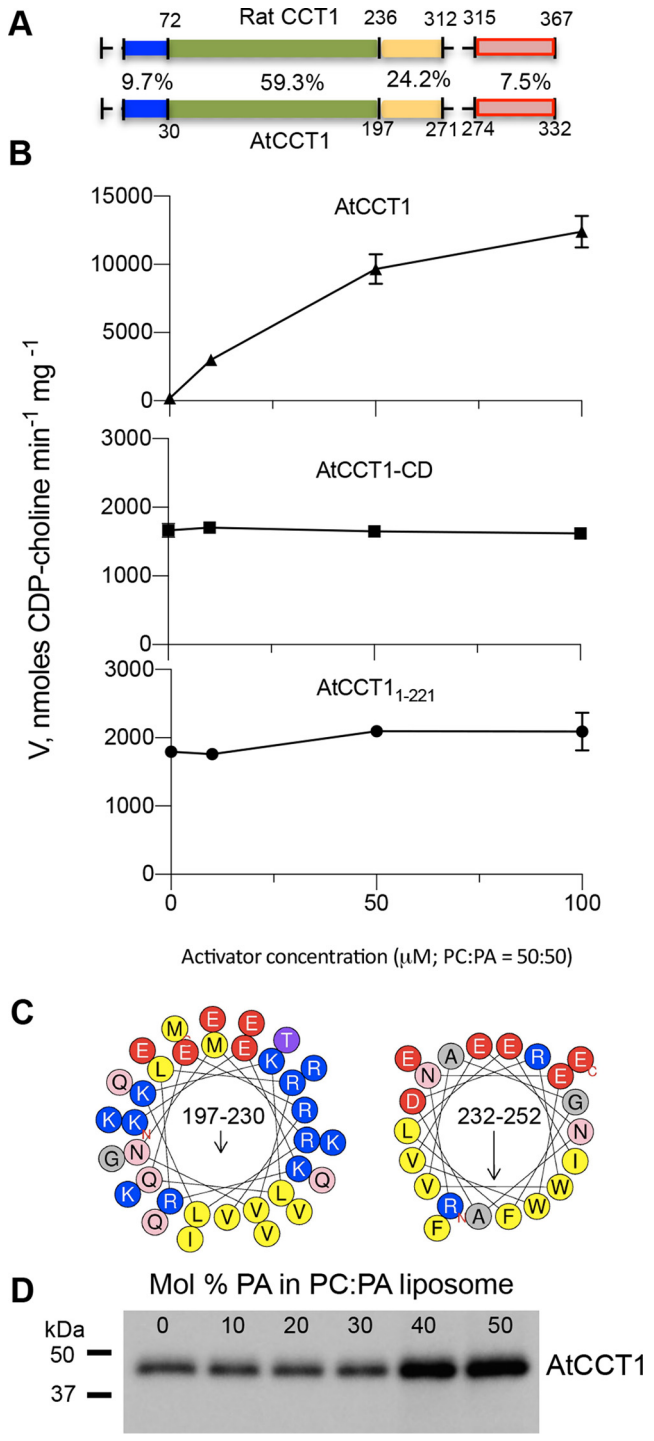

Figure 1. AtCCT1 has similar catalytic and membrane-binding domains as rat CCT1 but dramatically differs in the N- and C-terminal domains. *A*, the four major functional domains are shown for rat CCT1 and AtCCT1, and the percent sequence identity between domains from each species is indicated. The N-terminal region, catalytic domain, and membrane-binding domain are shown in *blue*, *green*, and *yellow*, respectively. The C-terminal domain, which corresponds to a phosphorylation domain in rat CCT1, is shown in *red*. *B*, initial velocity (*V*) of AtCCT1 and its truncated versions (*AtCCT1-CD/residues 1–197* and *AtCCT1* $_{1-221}$) in response to increasing PA concentration. Reported values are means ± S.D.; $n = 3$ technical replicates. *C*, helix wheel representation of the two segments of the membrane-binding domain that were identified by alignment with rat CCT1. Residues 197–230 can form amphipathic helices with a hydrophobic face, shown at the *bottom* in *yellow*. Residues 232–252, corresponding to the autoinhibitory motif in rat CCT1, can also form an amphipathic helix. *D*, a liposome binding study of AtCCT1 showed that it can interact weakly with the membranes, and this interaction was enhanced in response to increasing concentrations of PA. The bands corresponding to AtCCT1 were detected with an anti-HisG antibody in Western blotting.

residues. The corresponding autoinhibitory motif in AtCCT1 corresponds to residues 232–252 and can also form an amphiphatic helix, with the hydrophobic face composed of leucine, valine, phenylalanine, tryptophan, and isoleucine residues. To further probe the ability of AtCCT1 to interact with membranes, liposome binding studies were carried out, and the results showed that AtCCT1 can interact weakly with PC liposomes, and the interaction was enhanced in the presence of PA (Fig. 1*D*).

Homology modeling of AtCCT1 reveals highly conserved Rossmann fold and active-site residues

The structure of AtCCT1 was determined using SWISS-MODEL homology modeling. A rat CCT1 dimer structure (RCSB code 4MVC) (25) was used as a template because the catalytic form of the enzyme is a dimer (26). The predicted AtCCT1 homology structure shows a dimer, with each monomer consisting of the entire catalytic domain and a portion of the membrane-binding domain (Fig. 2*A*). This agrees with DISOPRED analysis predicting that the internal domain is likely to be well-folded. The covered sequence, which includes residue 30–216, has a sequence identity of 59.12% with the template, giving a good quality structural model with a QMEAN score of −2.01. The AtCCT1 catalytic domain has an α/β fold that follows a Rossmann fold, which is commonly observed in nucleotide-binding proteins (27). Specifically, as shown in Fig. 2*B*, this fold has five parallel β-strands (*green*, numbered *1–5* starting from the N terminus) that are connected by α-helices (*teal*, labeled *a–d*). The active-site residues identified in rat CCT1 were found to be highly conserved in AtCCT1; they include Lys-80, His-47, His-50, Arg-157, and Thr-163 (25, 28). These residues are localized near the region below the C-terminal portion of the parallel β-sheet (Fig. 2*C*) and line the wall of the catalytic pocket, as shown in the surface view (Fig. 2*D*). Below the catalytic pocket is the αE helix, which is located in the C-terminal part of the catalytic domain (Fig. 2, *A–C*, *dark blue*). Molecular dynamics simulation studies indicated that bending of the αE helices may be important for catalysis (29). The αE helix is followed by loops connecting to the membrane-binding domain. A portion of the membrane-binding domain (Fig. 2*A*, *yellow*) starts with a loop, followed by an α-helix interacting with the αE helix of the catalytic domain, indicating that the model exists as soluble inactive form.

Arabidopsis CCT1 lacks the C-terminal phosphorylation domain but is likely regulated via phosphorylation sites in the catalytic domain

The hydrophilic N-terminal region (Fig. 1*A*, *blue*) and the C-terminal domain of rat and *Arabidopsis* CCT1 (Fig. S1, *red*), unlike the core domains, are highly divergent, exhibiting only 9.7% and 7.5% sequence identity, respectively. Furthermore, DISOPRED analysis (30) indicated that the N- and C-terminal regions may have high propensity (close to a confidence score of 1.0) to be disordered in both animal and AtCCT1 (Fig. S4).

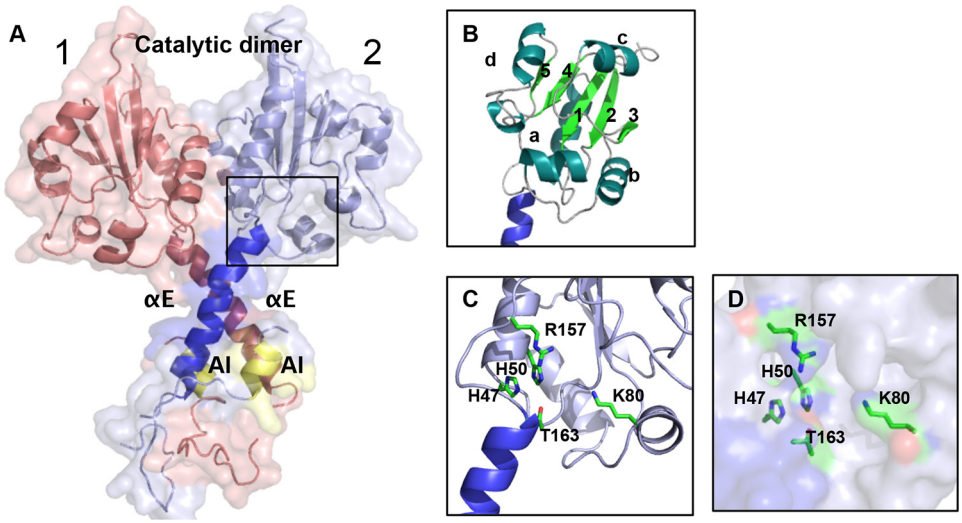

Figure 2. Homology modeling of AtCCT1 with the rat CCT1 structure as a template using SWISS-MODEL software. *A*, the model shows an AtCCT1 dimer; one monomeric catalytic domain is shown in *red* and the other one in *blue*. The *darker shades of blue* and *red* correspond to the αE helices, and the *yellow* part corresponds to a portion of the membrane-binding domain. *B*, close-up view of the Rossmann fold involved in nucleotide binding; five parallel β-sheets are shown in *green* (*1–5*), and the intervening α-helices are shown in *teal* (*a–d*). *C*, close-up view of the active site residues (Lys-80, His-47, His-50, Arg-157, and Thr-163) in the active site pocket (*boxed* in *A*) near the bottom part of the Rossmann fold. These residues were identified in rat CCT1 and found to be conserved in AtCCT1. *D*, surface view of the active-site pocket with the conserved active-site residues.

To further compare rat CCT1 and AtCCT1 structures, their N- and C-terminal regions were analyzed. Unlike the N terminus of rat CCT1, with a nuclear localization signal (31), the N-terminal region of AtCCT1 is shorter and contains no signal sequence (Fig. 1*A* and Fig. S1).

To explore the divergence and evolutionary relationship of plant and animal CCTs, a phylogenetic analysis was performed for CCTs from different organisms. CCTs from eudicots, monocots, and nonvascular plants diverged from their homologs from animal and yeast (Fig. 3*A*). Because most of the differences in the polypeptides are within the C-terminal domain, a detailed analysis of this portion was carried out. Animal and yeast CCTs are enriched with Ser and threonine residues in this region, whereas plant CCTs have a low abundance of these hydroxyl-containing amino acids (Fig. 3*A*). In addition, monocots have a much smaller C-terminal region relative to animal CCTs (Fig. 3*A*). These findings suggest that the evolution of this region is different between plants and mammals and might reflect different regulatory mechanisms. The C-terminal region of rat CCT1 corresponds to a phosphorylation domain containing 16 Ser and three Thr residues; 15 of these have been confirmed to be phosphorylated based on the PhosphoSite Plus database (Fig. 3*B*) (32). In contrast, the AtCCT1 C-terminal module only has three Ser and four Thr residues, with only one Ser residue being detected as a phosphorylation site (Ser-301) based on the PhosPhAt 4.0 database (Fig. 3*B*) (33). The AtCCT1 C-terminal domain is enriched in acidic residues with a pI of 3.79, whereas the pI of the rat CCT1 phosphorylation domain is 5.61 (Fig. 3*B*).

The phosphorylation domain mediates a major regulatory mechanism in mammalian CCT1 by influencing membrane affinity. Because this domain is apparently lacking in plant CCT1, it is possible that plant CCT1 is regulated via phosphorylation at sites in other domains of the enzymes. Closer inspection of the putative phosphorylation sites showed that Ser-187 is within a putative SnRK1 motif that has a consensus of (MLVFI)*X*(RKH)*XX*(ST)*XXX*(LFIMV), with Ser or Thr as the phosphorylation site (Fig. 3*C*). Another putative SnRK1 motif was detected at Ser-274. Ser-187 is within the catalytic domain, whereas Ser-274 resides at the beginning of the C-terminal domain (Fig. S1). Sequence alignment of AtCCT1 with nine homologs from other plant species showed that the Ser-187 phosphorylation consensus site within the catalytic domain is highly conserved whereas the one in the C-terminal domain (Ser-274) is not (Fig. 3*C*). This suggests that only Ser-187 is a functional consensus site that may be important in regulating CCT1 catalysis in various plant organisms. The putative SnRK1 site, Ser-187, was further mapped within the predicted three-dimensional structure of AtCCT1 (Fig. 3*D*). This site (Ser-187; Fig. 3*D*, *orange*) is localized in a loop region at the bottom of the αE helix (Fig. 3*D*, *blue*) and links the catalytic domain with the membrane-binding domain. Analysis of the structure showed that Ser-187 is present near the surface, which indicates that this residue is likely accessible to cytoplasmic enzymes involved in posttranslational modification (Fig. 3*D*). The possible importance of Ser-187 as a regulatory site is further corroborated by the fact that this site can be phosphorylated *in vivo* based on two independent nontargeted large-scale proteomic analysis of *Arabidopsis* proteins (34, 35).

AtCCT1 is phosphorylated by SnRK1, leading to enzyme inhibition

To test whether AtCCT1 can be phosphorylated by SnRK1, purified SnRK1 and AtCCT1 were assayed *in vitro* and subsequently analyzed through Phos-tag™ gel analysis and LC-MS/MS. Because SnRK1 needs to be activated by its activating kinase geminivirus Rep-interacting kinases (GRIK1/SnAK1), the SnRK1 kinase domain and GRIK1 were expressed in *E. coli* and partially purified using affinity chromatography (Fig. S2). SnRK1 was then activated through incubation with GRIK using

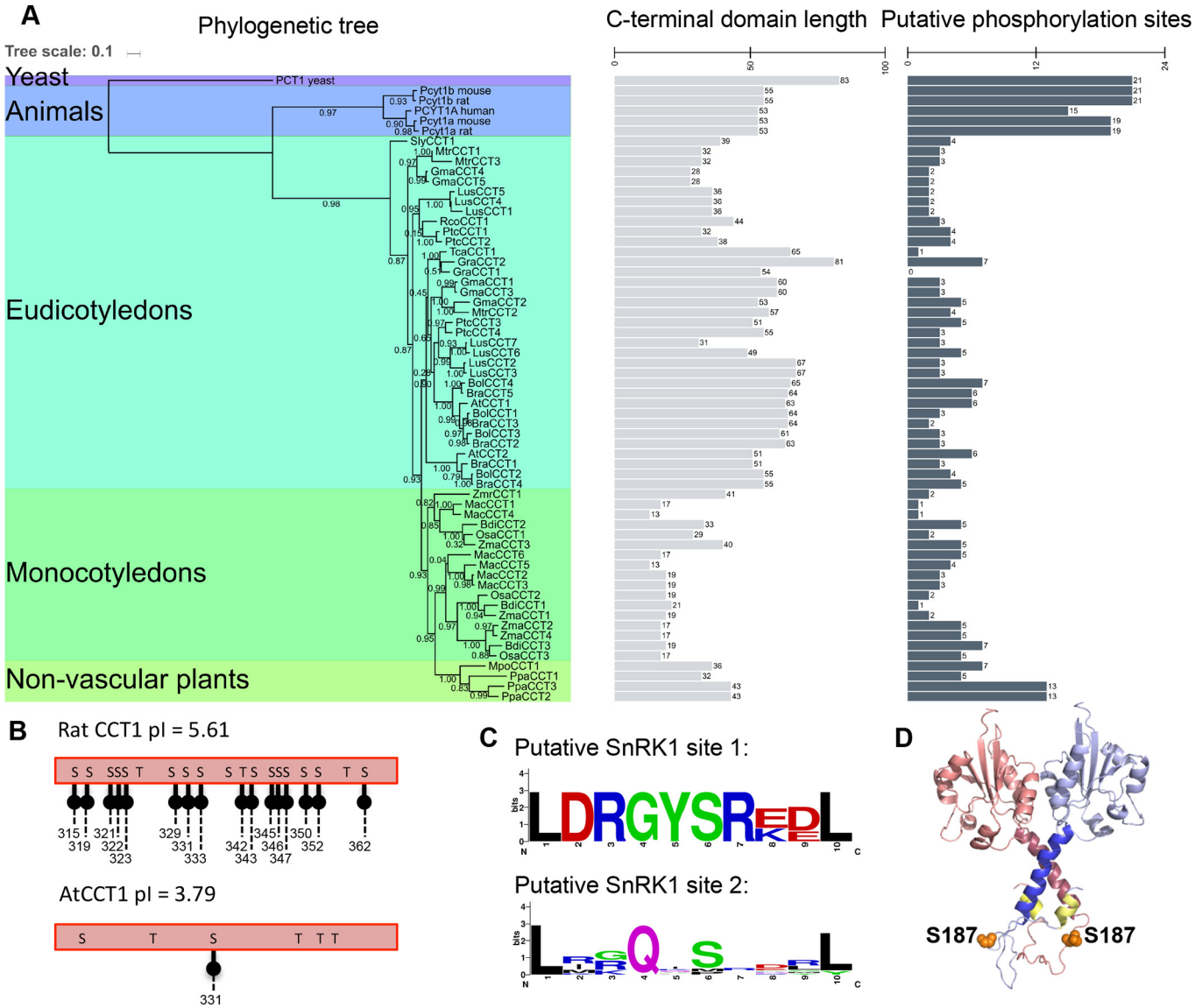

Figure 3. Evolutionary analysis of CCT, indicating that the C-terminal regulatory domain in plant CCT evolved differently than those of yeast and animal CCT, and identification of a novel putative regulatory phosphorylation site in plant CCT1. *A*, phylogenetic tree, length of the C-terminal region of CCT enzymes based on the alignment with the rat CCT, and the number of putative phosphorylation sites in the C-terminal domain. In animal CCT, the C-terminal region corresponds to a phosphorylation domain that is important for enzyme regulation. *B*, phosphorylation domain of rat CCT1 and the corresponding region in AtCCT1, showing the serine and threonine residues. The confirmed phosphorylated sites identified in proteomics studies based on the PhosphoSite Plus and PhosPhAt 4.0 databases are indicated by *lines* connected to *dots* with the corresponding residue numbers in the polypeptide. *C*, AtCCT1 and nine homologues were aligned to obtain the sequence logo for the two putative SnRK1 phosphorylation consensus (Ser-187 and Ser-274). The motif spanning Ser-187 is highly conserved, whereas the other one is not conserved. *D*, homology model structure of AtCCT1, showing the position of the highly conserved SnRK1 site (Ser-187).

a phosphorylation reaction reported previously and repurified (36). AtCCT1 was then incubated with increasing amounts of activated SnRK1 (0–47 pmol), and the phosphorylation state of the enzyme was analyzed through Phos-tag™ gel electrophoresis. In this analysis, phosphorylated proteins exhibit a shift in mobility because of the presence of a phosphate-binding tag. The protein was then detected by Western blotting using anti-His_6 HRP. In the absence of SnRK1, AtCCT1 formed one band, indicating the absence of any phosphorylated protein (Fig. 4*A*). Upon addition of SnRK1, the intensity of the unphosphorylated band was reduced, accompanied by simultaneous formation of higher-molecular-weight bands, indicating that AtCCT1 was phosphorylated.

To probe the effect of AtCCT1 phosphorylation on enzyme activity, AtCCT1 was preincubated with increasing amounts of activated SnRK1, and the activity was subsequently determined in the presence of PC:PA vesicles. AtCCT1 incubated in kinase buffer without SnRK1 was used as a reference. It was found that addition of small amounts (2.5 pmol) of activated SnRK1 resulted in decreased AtCCT1 activity by about 15% to 25% (Fig. 4*B* and Fig. S5). The AtCCT1 activity further decreased with addition of increasing amounts of SnRK1. A maximal decrease of about 70% in AtCCT1 activity was observed in the presence of the highest amount of SnRK1 (47 pmol). The plot is a result of three enzyme activities; specifically, GRIK phosphorylation of SnRK1, SnRK1 phosphorylation of AtCCT1, and

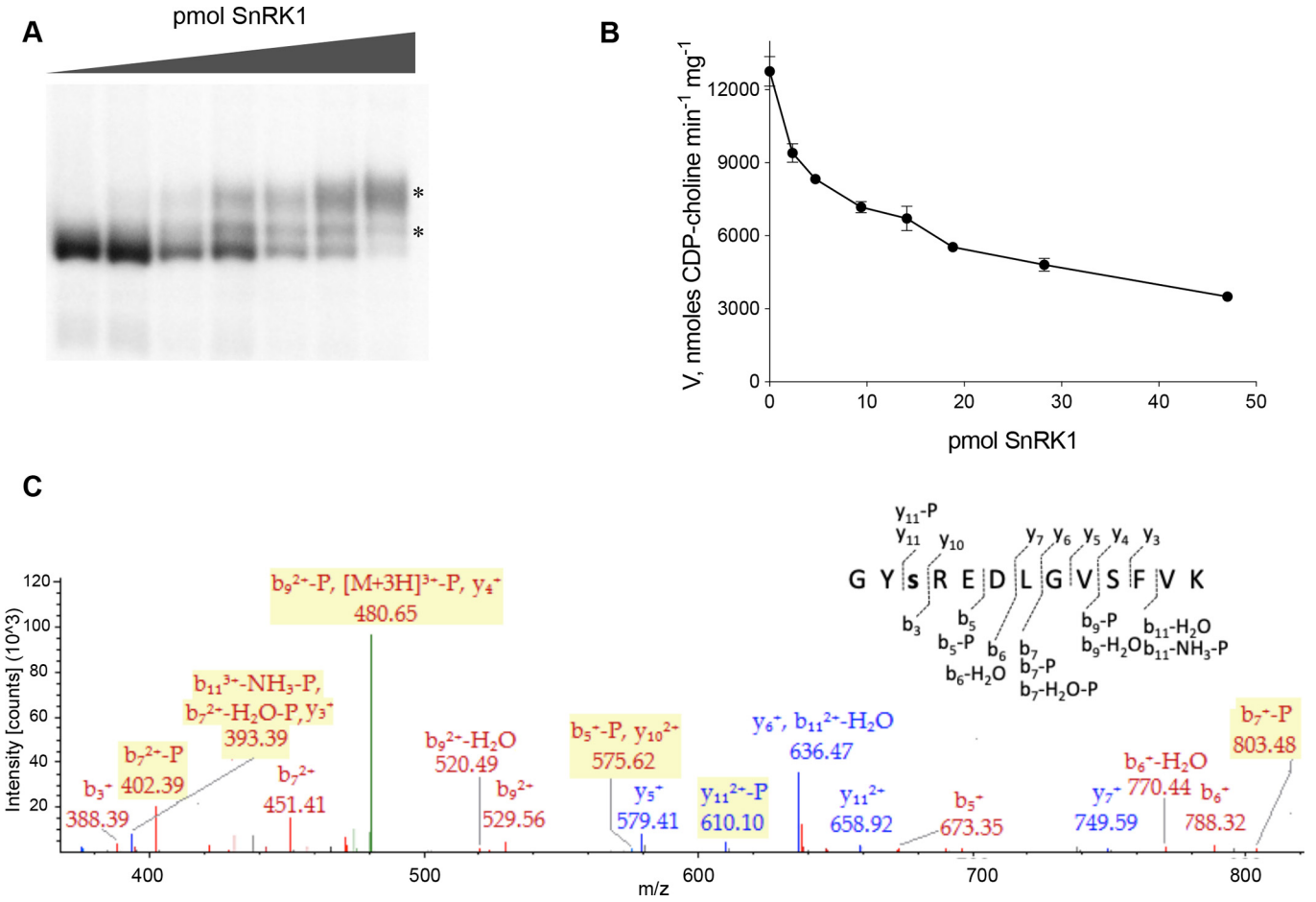

Figure 4. SnRK1 phosphorylation of AtCCT1. *A*, Phos-tag™ gel analysis of AtCCT1 with increasing amounts of SnRK1 (0, 2.4, 4.7, 9.4, 18.8, 28.2, and 47.0 pmol). The lowest band corresponds to unphosphorylated AtCCT1. The upper bands (*asterisks*) are the phosphorylated forms of AtCCT1. *B*, kinetics analysis of CCT1 treated with increasing amounts of SnRK1 in the presence of PC:PA vesicles. Addition of increasing amounts of SnRK1 resulted in lower CCT activity, indicating that phosphorylation inhibits the enzyme. Reported values are means ± S.D.; $n = 3$ technical replicates. *C*, MS/MS fragmentation pattern of the phosphorylated peptide GYsREDLGVSFVK in AtCCT1 after SnRK1 treatment, showing the presence of phosphorylated Ser-187 (*lowercase s*). The triply charged phosphorylated form of the aforementioned peptide has a theoretical *m/z* of 512.9031 (mono)/513.2053 (av), and the parent ion of the detected peptide had an *m/z* of 512.9090. The peptide sequence with the corresponding y and b ions is shown as an *inset*. Phosphorylation of Ser-187 is indicated by the parent ion *m/z* and the adequate sequence coverage for y3, y4, y5, y6, y7, y10, y11, b3, b5, b6, b7, b9, and b11 spectral lines.

AtCCT1 activity. Three biological replicates are shown in Fig. S5. The result clearly indicates that SnRK1-mediated phosphorylation of AtCCT1 resulted in conversion of AtCCT1 into an inactive conformation.

To identify the phosphorylation site, SnRK1-treated AtCCT1 was subjected to in-gel trypsin digestion coupled with LC-MS/MS sequencing. A percent coverage of 79.86% was obtained during sequencing, including the peptide GYsREDLGVSFVK, which contains the predicted SnRK1 phosphorylation site Ser-187. Indeed, all peptide fragments detected for this sequence had the phosphorylated Ser-187 residue, indicating that SnRK1 efficiently phosphorylated this site (Fig. 4*C*). Phosphorylation at the other predicted SnRK1 site, Ser-274, however, could be detected in the current experiment, as no peptide fragment containing this site was found. It should be noted that Ser-274 was also not identified as a phosphorylation site in two large-scale proteomics analyses of *Arabidopsis* proteins in previous studies (34, 35), suggesting that this site may not be involved in posttranslational regulation. Interestingly, SnRK1 was found to phosphorylate AtCCT1 at another site (Ser-194). This site is three residues away from the SnRK1 consensus peptide sequence and is phosphorylated to a much lesser extent than Ser-187. Moreover, of the 50 peptide spectral matches having phosphorylated Ser-187, only eight matches also had phosphorylated Ser-194. Therefore, Ser-194 is likely not a preferred site for SnRK1 phosphorylation. In addition, the other phosphorylated site (Ser-301) detected in past proteomics analyses (34, 35) was not phosphorylated after SnRK1 treatment, indicating that another kinase might act at that site.

Phosphorylation at Ser-187 appears to directly affect the catalytic domain and thus inhibits AtCCT1

To probe the biochemical mechanism of AtCCT1 inhibition by SnRK1-mediated phosphorylation, we further investigated the effect of SnRK1 on AtCCT1-CD, which only contains one major SnRK1 phosphorylation site, Ser-187. Phosphorylation of AtCCT1-CD by SnRK1 was monitored using LC-MS/MS. Of the 131 spectral masses detected for peptides with Ser-187, only 26 also had the phosphorylated Ser-194, which confirmed that SnRK1-mediated phosphorylation mainly occurs at Ser-187 (Fig. 5*A*). The MS/MS spectrum of the diphosphorylated peptide with Ser-187 and Ser-194 is shown in Fig. S6. AtCCT1

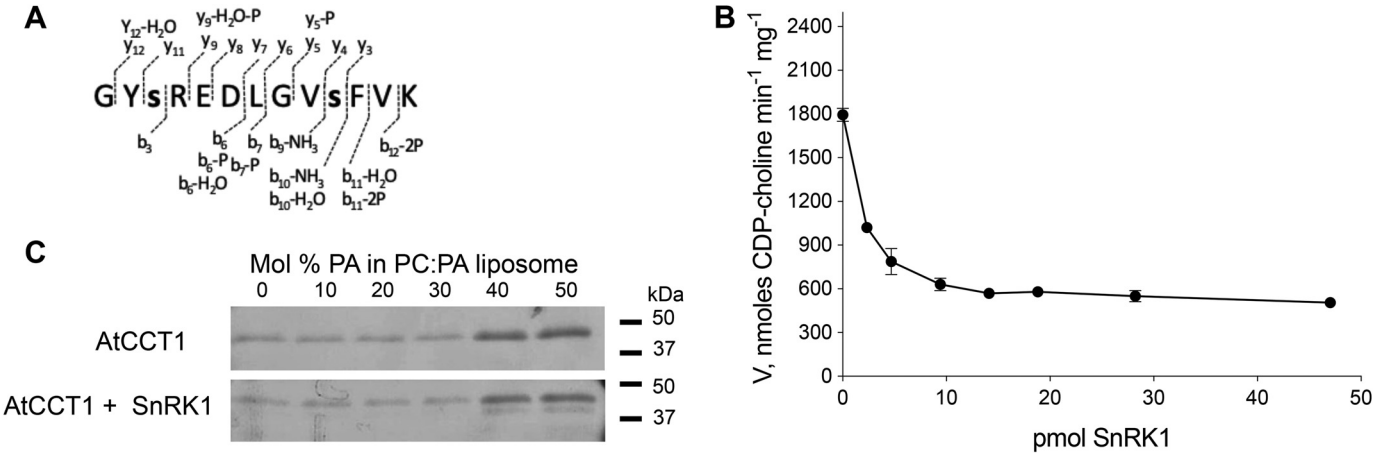

Figure 5. SnRK1 phosphorylation and kinetics analysis of AtCCT1-CD. *A*, peptide sequence showing the MS/MS fragmentation pattern of the AtCCT1-CD peptide (GYsREDLGVsFVK), showing that SnRK1 phosphorylates AtCCT1-CD at Ser-187 and Ser-194. The MS/MS spectrum for this diphosphorylated peptide is shown in Fig. S6. *B*, phosphorylation of Ser-187 within the catalytic site is sufficient to lower the activity of the enzyme. Reported values are means S.D.; $n = 3$ technical replicates. *C*, liposome binding assay of AtCCT1 with and without treatment with SnRK1. SDS-PAGE shows that phosphorylated AtCCT1 can still bind to PA-enriched membranes. Phosphorylated AtCCT1 forms an upper band during electrophoresis.

contains 27 other Ser and Thr residues, but no other off-site phosphorylation was observed. Moreover, the effect of phosphorylation on enzyme activity was also determined (Fig. 5*B*). Because PC:PA vesicles had no effect on the activity of AtCCT1-CD (Fig. 1*B*), these lipids were not added in this assay. Addition of 2.5 pmol SnRK1 was able to lower the enzyme activity by about 40%. In the absence of the C-terminal region following the catalytic domain, the SnRK1 phosphorylation site is most likely more accessible for phosphorylation than that in the full-length enzyme. A further increase in SnRK1 concentration led to a substantial decrease in enzyme activity by about 70%. In addition, a liposome binding assay was carried out to determine whether phosphorylation can prevent AtCCT1 from binding to the membrane, as in the case of interference of phosphorylation in the C-terminal domain of rat CCT1 (21, 37). SnRK1-treated AtCCT1 formed two bands in SDS-PAGE, with the top band corresponding to the phosphorylated form, as confirmed by LC-MS/MS (Fig. 5*C*). Phosphorylated AtCCT1 could still interact with PA-enriched liposomes, indicating that the SnRK1 modification did not interfere with membrane interaction (Fig. 5*C*).

The importance of Ser-187 was further investigated by mutation to alanine. The S187A variant was found to have a specific activity of 4032 nmol CDP-choline min^{-1} mg $protein^{-1}$, which is 67% lower than that of the native enzyme, indicating the importance of this serine residue in maintaining the active conformation of the enzyme (Fig. 6*A*). The effect of SnRK1 phosphorylation on S187A was then probed, and it was found that this variant is less susceptible to SnRK1 inhibition compared with the native enzyme (Fig. 6*B*). These results clearly indicate that Ser-187 is the major target of SnRK1 phosphorylation in AtCCT1. The substrate saturation curve of AtCCT1 was then compared with the phosphorylated form of the enzyme. As shown in Fig. 6*C*, SnRK1 phosphorylation of AtCCT1 decreased the V_{max} and increased the $K_{0.5}$, indicating that phosphorylation favors the low-affinity state of the enzyme.

Transient expression of AtCCT1-CD and SnRK1 in N. benthamiana leaves represses AtCCT1-induced PC biosynthesis

The effect of SnRK1-mediated phosphorylation on AtCCT1 was further probed *in planta* through transient expression in *N. benthamiana* leaves. Previously, it has been shown that expression of *AtCCT1* in *Arabidopsis* had no effect on PC levels, whereas expression of cDNA encoding the catalytic domain alone (AtCCT1-CD) was able to drive higher PC accumulation in *Arabidopsis* roots (6). Moreover, MS analysis, protein truncation, and liposome binding studies indicated that AtCCT1 is phosphorylated and inhibited by SnRK1 in the catalytic domain. Therefore, *AtCCT1-CD* and *SnRK1* were transiently coexpressed in tobacco leaves. The amount of PC was then isolated and quantified. Consistent with previous observations in *Arabidopsis* roots, the transient expression of *AtCCT1-CD* in tobacco leaves was able to drive PC content to higher levels compared with the control injected with the *p19* vector (Fig. 7). Coexpression of *SnRK1* with *AtCCT1-CD*, however, resulted in lower PC levels than overexpression with *AtCCT1-CD* alone, indicating that SnRK1 can inhibit AtCCT1 *in planta*. It was further noted that expression of *AtCCT1-CD* with and without *SnRK1* did not affect the fatty acid composition of PC compared with the control (Fig. 7).

Discussion

PC biosynthesis involves a series of reactions consuming carbon and energy, but it remains unclear how this highly endergonic process is fine-tuned with energy homeostasis. Here we identify a mechanistic link between SnRK1, an important energy sensor kinase, and CCT1, the enzyme catalyzing a key regulatory step in PC formation. SnRK1 has been shown to phosphorylate and concomitantly inhibit CCT1. SnRK1 has been shown previously to modulate the biosynthesis of various cellular compounds in response to the global energy state in cells, including carbohydrates, amino acids, isoprenoids, and storage lipids (10, 15, 17). Our findings dem-

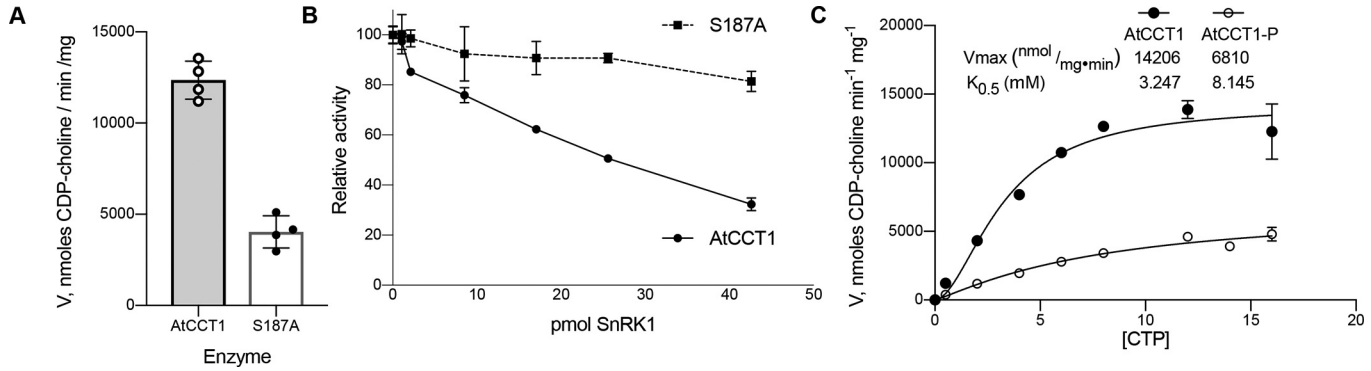

Figure 6. Probing the possible mechanism of inhibition. *A*, specific activity of S187A compared with native AtCCT1. Reported values are means ± S.D.; $n = 4$ technical replicates *B*, effect of incubation of increasing amounts of SnRK1 on the S187A variant compared with WT AtCCT1. *C*, CTP saturation curve of AtCCT1 and AtCCT1 treated with SnRK1 (*AtCCT1-P*). Data were fitted using the allosteric sigmoidal model, and the R^2 values were 0.94 and 0.95 for AtCCT1 and AtCCT1-P, respectively. Reported values are means ± S.D.; $n = 3$ technical replicates. The assays were carried out in the presence of PC:PA vesicles.

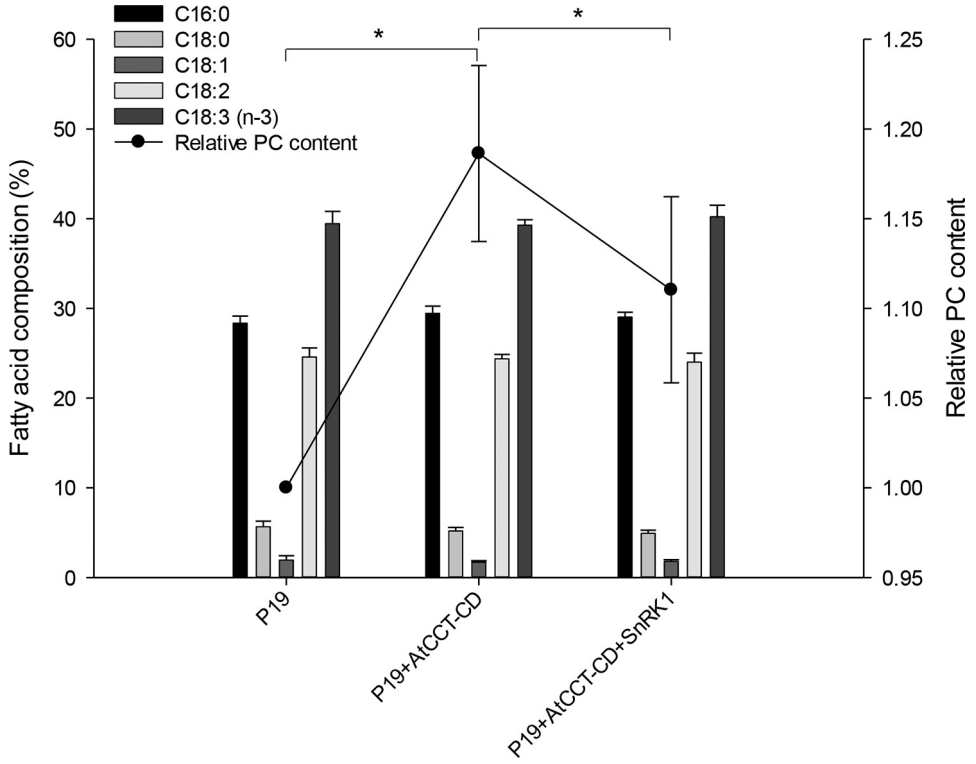

Figure 7. Effect of transient expression of *AtCCT1-CD* and *SnRK1* in *N. benthamiana* leaves on PC content. *Agrobacterium*-mediated-expression of *P19* (empty vector control), *P19* + *AtCCT1-CD*, and *P19* + *AtCCT1-CD* + *SnRK1* in tobacco leaves was carried out, and relative PC content was determined. The values are means ± S.E., $n = 5$. *, $p < 0.05$ as determined by paired one-tailed *t* test.

onstrated that SnRK1 is also involved in the regulation of plant PC biosynthesis.

Because little information is available regarding the regulation of plant CCT, the structure and biochemical regulation of AtCCT1 were analyzed in detail and compared with the well-studied rat CCT1. Mammalian CCT has four functional domains: the N-terminal signal for nuclear transport, catalytic core, membrane-binding regulatory domain, and C-terminal phosphorylation module (Fig. 1) (2). The catalytic core is highly conserved between AtCCT1 and rat CCT1, with a sequence identify of 59.3% (Fig. 1), and has the H*X*GH motif, implicated in CTP binding and stabilization of the transition states (38). Homology modeling predicted that the Rossmann fold of the catalytic domain as well as the locations and identities of active-site residues are conserved in both rat and plant CCT1 (Fig. 2). The Rossmann fold serves as a structural motif that binds nucleotides and may be expected to bind the cytidyl moiety of CDP-choline as in rat CCT1 (29, 27). It should be noted that the proposed AtCCT1 structure was modeled based on a rat CCT1 dimer structure (25). Because the oligomeric nature of AtCCT1 remains unknown, it would be interesting to further pursue a detailed structural characterization study in the future. The AtCCT1 catalytic domain is succeeded by the membrane-binding domain, which exhibits 24.2% sequence identity with rat CCT1 (Fig. 1). The membrane-binding domain of rat CCT1 modulates CCT activity through amphitropism by weakly and reversibly binding to membranes (39). This domain has an autoinhibitory motif that forms an α-helix that interacts with

another helix located at the bottom part of the catalytic domain, and the interaction blocks access to an important catalytic lysine residue in rat CCT1 (25). Autoinhibition could be relieved upon interaction of the membrane-binding domain with membranes that are enriched in DAG, PA, and free fatty acids (39–41). In the absence of activating lipids, AtCCT1-CD and AtCCT1$_{1-221}$ are more active than full-length AtCCT1, suggesting the presence of an inhibitory region. AtCCT1-CD, however, is only about 15% active as a full-length enzyme at 50 μM PA:50 μM PC vesicles, suggesting that the membrane-binding domain may have a more prominent activating function in the presence of PC:PA vesicles. This property is similar to that of the animal CCT1 membrane-binding domain, which has been found to have inhibitory and activating functions (24). These findings are consistent with the previous *in planta* observation that AtCCT1 is specifically activated by increased PA (6). Thus, it is likely that AtCCT1 functions as a metabolite sensor that helps maintain membrane homeostasis by generating PC when other compounds affect the membrane structure.

Although plant CCT contains the conserved catalytic domain and the amphipathic membrane-binding domain, high sequence divergence can be observed between the N- and C-terminal regions of animal and plant CCTs (Fig. 1). Indeed, plant CCT1 does not contain the N-terminal nuclear transport signal or the C-terminal phosphorylation domain as animal CCT1 does (Fig. 1). Instead, the C-terminal domain of AtCCT1 only has one detected phosphorylated Ser site (Fig. 3). Sequence alignment of plant CCT1 from various species showed that the lesser prevalence of Ser residues within this domain is common among the plant gene family (Fig. 3). This structural property is quite different from the C-terminal phosphorylation domain of mammalian CCT, which contains multiple phosphorylation sites and contributes to the fine-tuning of enzyme activity through interaction with anionic lipids (21). In addition, phosphorylation of mammalian CCT modulates the affinity of the enzyme with membranes, as addition of the phosphoryl groups favors the soluble inactive state (37). Furthermore, DISOPRED analysis of both plant and animal C-terminal modules showed their highly disordered nature (Fig. S4). For this reason, this domain is usually not captured in reported crystal structures of the rat enzyme (25). Long disordered regions have been reported to exhibit a high evolutionary rate leading to high sequence variability (42). Although it is apparent that the plant C-terminal domain does not function as a multiphosphorylation module, this domain may have other regulatory functions, as disordered regions have been increasingly recognized for their role in regulation and cellular signaling (43).

Because the C-terminal phosphorylation domain in animal CCT that plays a role in enzyme regulation is missing in plant CCT, the latter may operate under different regulatory mechanisms. Phosphorylation of AtCCT1 was identified to occur within the catalytic domain at Ser-187 by SnRK1 (Fig. 4), whereas mammalian CCT phosphorylation was mainly localized within the phosphorylation domain (20). Unlike the mammalian CCT, SnRK1 phosphorylation at this site does not seem to affect the localization of this enzyme between the membrane-bound and soluble states. Instead, SnRK1-mediated phosphorylation of AtCCT1 directly inhibited the enzyme up to 70% *in vitro* (Fig. 4). Consistently, SnRK1 phosphorylation of AtCCT1-CD has the same effect as phosphorylation of the full-length enzyme (Fig. 5). It should be noted that a smaller amount of SnRK1 was able to achieve the maximal decrease in AtCCT1-CD activity, indicating that Ser-187 may be more accessible in the absence of the membrane-binding and phosphorylation domains. In addition, SnRK1 phosphorylation of AtCCT1 did not affect the affinity for the membrane (Fig. 5*C*). These results are further supported by our transient expression results, in which coexpression of *SnRK1* and *AtCCT1-CD* led to decreased PC accumulation in tobacco leaves compared with expression of *AtCCT1-CD* alone (Fig. 7).

Similar to AtCCT1, HMG-CoA reductase is also phosphorylated by SnRK1 at a Ser residue (Ser-577), which is localized within the catalytic domain (44). SnRK1 phosphorylation at this site was able to reduce the activity of purified HMG-CoA reductase by more than 80%. This Ser residue was six residues away from a key histidine residue that acts as an acid–base catalyst during catalysis. Phosphorylation of Ser-577 has been proposed to hinder the histidine residue from donating a proton to one of HMG-CoA's substrates. As for a nitrate reductase, the SnRK1 phosphorylation site is within a hinge region between a cytochrome *b* domain and a molybdenum cofactor-binding domain, and phosphorylation has been proposed to block the electron transfer needed for the reduction reaction (45). As for AtCCT1, the SnRK1 sites is located at the bottom of the αE helix (Fig. 3*D*). This helix has been found to exhibit varying conformations during catalysis, based on detailed molecular dynamic simulations (29). It is possible that phosphorylation of Ser-187 can directly influence the conformation of the αE helix, thereby affecting activity. The importance of Ser-187 in maintaining an active enzyme conformation was further confirmed, as mutation of this residue to alanine reduced enzyme activity. The lower V_{max} and higher $K_{0.5}$ of SnRK1-phosphorylated AtCCT1 further confirmed this hypothesis. Future work may involve structural characterization of native and SnRK1-phosphorylated AtCCT1 to assess the exact conformational change or constraint brought about by phosphorylation.

The current findings further affirmed our previous observation that DGAT1 and CCT1 exhibit a similar mode of regulation. Both enzymes have autoinhibitory motifs within a region with high propensity to become disordered, are activated by PA, and are substrates of SnRK1 (6, 17). In plants, TAG is mainly stored in the form of lipid bodies, which are composed of TAG surrounded by a monolayer of PC molecules (46). Coactivation and coinhibition of CCT1 and DGAT1 may have important physiological roles to enable PC biosynthesis to keep pace with TAG and lipid body production. SnRK1-mediated inhibition of CCT1 and DGAT1 also provides a link between sugar/energy homeostasis and lipid biosynthesis, in which lipid biosynthesis is favored when SnRK1 is inhibited by high intracellular sugar levels; conversely, lipid biosynthesis is curtailed because of activation of SnRK1 by low sugar levels.

Based on the results of this study and previous studies, a diagram of the regulatory role of SnRK1 in plant lipid biosynthesis was generated (Fig. 8). The carbon precursors for phospholipid and TAG biosynthesis are mainly derived from sugar flux through glycolysis and fatty acid biosynthesis. As an energy

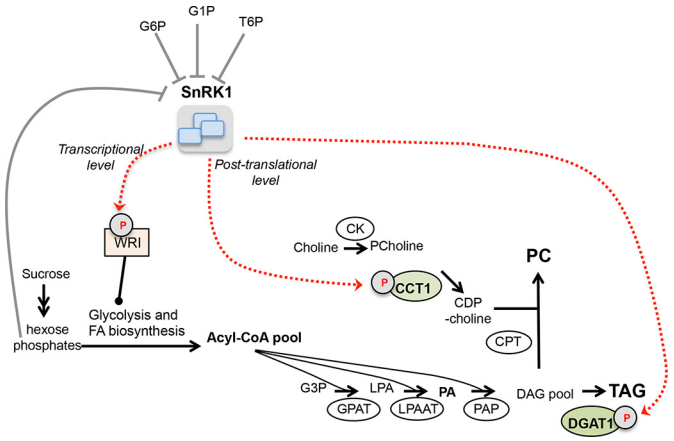

Figure 8. SnRK1 regulates plant lipid biosynthesis at the transcriptional and posttranslational levels. At the transcriptional level, SnRK1 regulates the stability of WRI, which is a transcription factor modulating the expression of glycolytic and lipid biosynthetic genes. At the posttranslational level, SnRK1 can phosphorylate and inhibit CCT1 and diacylglycerol acyltransferase 1 (DGAT1), which are key regulatory enzymes in PC and TAG biosynthesis, respectively. SnRK1 is allosterically regulated by various hexose phosphates (glucose-6-phosphate (*G6P*), glucose-1-phosphate (*G1P*), and trehalose-6-phosphate (*T6P*)) and provides a link between lipid biosynthesis and sugar/energy homeostasis. *CK*, choline kinase; *CPT*, choline phosphotransferase, *G3P*, *sn*-glycerol-3-phosphate; *LPA*, lysophosphatidate; *FA*, fatty acid; *GPAT*, *sn*-glycerol-3-phosphate acyltransferase; *LPAAT*, lysophosphatidic acid acyltransferase; *PAP*, phosphatidic acid phosphatase; *PCholine*, phosphocholine.

sensor kinase, SnRK1 is regulated by sugar levels; glucose-6-phosphate, trehalose-6-phosphate, and glucose-1-phosphate act as allosteric inhibitors of the kinase (16, 47–49). Recent findings show that SnRK1 ensures that the rate of lipid biosynthesis is adjusted based on available sugar both at the transcriptional and posttranslational levels. Specifically, SnRK1 modulates transcription of glycolytic and fatty acid biosynthetic genes via WRI1 (15). Phosphorylation of WRI1 facilitates its degradation, which leads to lower gene expression levels of lipid biosynthetic genes. At the posttranslational level, SnRK1 directly phosphorylates and inhibits CCT1 and DGAT1, which are key enzymes in PC and TAG biosyntheses, respectively (17). This observation is similar to the regulatory role of SnRK1 in carbohydrate metabolism at the transcriptional and posttranslational levels (10).

Conclusions

This study found that AtCCT1 has highly conserved structural fold and active site motifs as rat CCT1 does but lacks the regulatory C-terminal phosphorylation domain. Instead, AtCCT1 has a phosphorylation site within the catalytic domain, which is regulated by SnRK1. The results identified a possible link between *de novo* PC biosynthesis and energy homeostasis because SnRK1 serves as an energy sensor kinase regulating various biosynthetic pathways. SnRK1 can phosphorylate AtCCT1 at Ser-187, which leads to a substantial reduction in AtCCT1 activity. Phosphorylation appears to directly influence the catalytic domain and does not interfere with PA-mediated activation of AtCCT1. These findings are further supported by the results of *N. benthamiana* transient leaf expression, which showed that coexpression of *AtCCT1-CD* with *SnRK1* led to lower PC levels than expression of *AtCCT1-CD* alone. The highly conserved nature of the SnRK1 consensus site indicates that this mode of CCT1 regulation may also operate in other plants. Taken together, our results indicate that SnRK1 regulates the activity of AtCCT1, which provides a mechanistic link between sugar/energy homeostasis and the *de novo* PC biosynthesis.

Experimental procedures

Sequence analysis and structural homology modeling analysis of CCT1

Sequence alignment was performed using Clustal Omega. The proteomic phosphorylation profiles of rat CCT1 (UniProt ID P19836) and AtCCT1 (UniProt ID Q9ZV56) were obtained from the PhosphoSite Plus (32) and PhosPhAt 4.0 (33) databases, respectively. The sequence logo of the SnRK1 consensus sites from AtCCT1 and nine other homologues were obtained using the Weblogo server (http://weblogo.berkeley.edu/logo.cgi).[4] The plant CCT1 sequences and their corresponding UniProt accession numbers are *A. thaliana* (Q9ZV56), *Capsella rubella* (R0FX10), *Eutrema salsugineum* (V4M9M2), *Noccaea caerulescens* (A0A1J3DQT0), *Brassica napus* (Q42619), *Populus tomentosa* (A0A1L6K5N4), *Arabis alpina* (A0A087HL73), *Punica granatum* (A0A218X9E1), *Citrus sinensis* (A0A067FAG2), and *Populus trichocarpa* (A0A2K1ZUV0). A detailed description of the methods used to reconstruct phylogenetic tress can be found in (Methods S1 and Table S1). Three-dimensional modeling of AtCCT1 was performed using SWISS-MODEL and viewed using PyMOL. DISOPRED3 was used to predict the degree of disorder of the different domains (50).

Production and purification of recombinant AtCCT1, AtCCT1-CD, and AtCCT1$_{1–221}$

The *Arabidopsis CCT1* cDNA sequence was codon-optimized for recombinant expression in *E. coli* and purchased from General Biosystems, Inc. The cDNA sequences corresponding to AtCCT1, AtCCT1-CD, and AtCCT1$_{1–221}$ were cloned into the pET16b vector with a modified His$_6$ N-terminal tag. The AtCCT1-S187A mutant was generated using a two-step PCR method with AtCCT1 cDNA as a template and cloned in the same vector. The BL21 (DE3)– competent *E. coli* strain (New England Biolabs) transformed with the plasmid was grown overnight at 37 °C in 25 ml of Luria broth medium with 100 μg/ml ampicillin (LB-Amp). The overnight culture (15 ml) was then used to inoculate 1 liter of fresh LB-Amp, which was grown to an A_{600} of 0.6. Recombinant protein expression was induced by addition of 0.8 mM isopropyl β-D-thiogalactopyranoside, followed by incubation at 22 °C for 16 h. The cell pellet was recovered by centrifugation, stored at −20 °C for at least 1 h, and mixed with 40 ml of lysis buffer (50 mM Tris-HCl (pH 8.0), 150 mM NaCl, and 1% Triton X-100). The cells were sonicated six times at 75% power (with a 10-s on and 10-s off cycle) for a total of 10 min. The cell lysate was spun at 25,000 × *g* for 20 min, and the supernatant was incubated with 0.5 ml of Ni-NTA (Thermo Scientific). The resin was recovered by passing through a fritted glass column and washed with 40 column

[4] Please note that the JBC is not responsible for the long-term archiving and maintenance of this site or any other third party–hosted site.

volumes of lysis buffer. The protein was obtained by elution in 3 ml of lysis buffer containing 500 mM imidazole.

CCT activity assay

CCT activity was analyzed with a method reported previously (22). Other than described, the reaction was carried out in a 100-μl reaction mixture containing 50 mM imidazole, 25 mM magnesium acetate (pH 7.0), 10 mM CTP, 4 mM phosphocholine chloride calcium salt tetrahydrate, and 50 μM PC:50 μM PA vesicles. These compounds were purchased from Sigma-Aldrich. The reaction was started by addition of CCT1 protein, followed by incubation at 37 °C for 15 min. The reaction was stopped by incubation in boiling water for 5 min. After boiling, the samples were centrifuged at 16,000 $\times$ *g* for 10 min to remove precipitated materials, and 50 μl of supernatant was diluted in 450 μl of distilled water in 12 $\times$ 32 mm glass vials. The amount of CDP-choline formed was quantified using HPLC (Agilent 1260 Infinity equipped with a diode array detector and a Zorbax C18 (Aq) 4.6 mm x 15 cm column). From the 500-μl diluted reactions, 10 μl was injected into HPLC via an autosampler. The mobile phase consisted of 0.10 M ammonium bicarbonate (98%) and acetonitrile (2%) (pH 7.4), which was used to equilibrate the column for 15 min. An isocratic flow rate of 0.5 ml/min per sample/standard was used. The CTP and CDP-choline signals were obtained using UV absorbance at 254 nm for the cytosine ring. The data were examined using the Openlab program. A calibration plot was made with serial dilution of the CDP-choline standard (0.001–0.1 mM). The plot of the peak area as a function of CDP-choline concentration was used to calculate CDP-choline content in the sample. The substrate saturation curves were fitted with model equations using GraphPad Prism 7.0a.

Phosphorylation of AtCCT1 by Arabidopsis SnRK1 and analysis of the phosphorylated enzyme

The SnRK1.1 kinase domain (UniProt ID Q38997; KIN10) with a His_6 tag and GRIK1 (UniProt ID Q93V58) with a GST tag were overexpressed in *E. coli* BL21 and purified using Ni-NTA and GSH-Sepharose affinity chromatography, respectively, as described previously (36). To activate SnRK1, it was incubated with GRIK1 in a standard phosphorylation reaction, repurified, and stored in NTA-Ni elution buffer supplemented with 1 mM DTT in 50% glycerol. Purified AtCCT1 and AtCCT1-CD were incubated with activated SnRK1 in a 45-μl reaction volume in kinase buffer (50 mM Tris-HCl (pH 7.5), 10 mM $MgCl_2$, 1 mM DTT, and 1 mM EDTA), 200 μM ATP, and 5 μl (5 μg) substrate at 30 °C for 30 min. Subsequently, the AtCCT1 enzymes were assayed using 5 μl of the treated enzyme in the CCT assay described above. The phosphorylation state of the enzyme was analyzed by resolving through 7.5% SuperSep™ Phos-tag™ gel using prechilled running buffer to minimize band diffusion. When the dye reached the bottom, the resolved proteins were blotted on a PVDF membrane. AtCCT1 and the phosphorylated enzymes were then detected using anti-HisG-HRP antibody (Thermo Fisher Scientific, product 46-1009, lot 1923164) coupled with the ECL detection system (Amersham Biosciences).

In-gel trypsin digestion coupled with LC-MS/MS

AtCCT1 was first treated with SnRK1 under standard reaction conditions. It was then resolved through SDS-PAGE, and the AtCCT1 band was excised and subjected to in-gel trypsin digestion. Briefly, the excised gel band was destained in 100 mM ammonium bicarbonate/acetonitrile (50:50), reduced in 10 mM β-mercaptoethanol in 100 mM bicarbonate, and alkylated with 55 mM iodoacetamide in 100 mM bicarbonate. The gel pieces were then dehydrated, covered with trypsin (6 ng/μl), and incubated overnight (~16 h) at room temperature. The peptides were extracted twice from the gel using 97% water/2% acetonitrile/1% formic acid, followed by 50% of the first extraction buffer and 50% acetonitrile. The recovered tryptic peptides were resolved and ionized using nanoflow HPLC (Easy-nLC II, Thermo Scientific) coupled to an LTQ XL-Orbitrap hybrid mass spectrometer (Thermo Scientific). Nanoflow chromatography and electrospray ionization were carried out using a PicoFrit fused silica capillary column (ProteoPepII, C18) with a 100-μm inner diameter (300 Å, 5 μm, New Objective). The sample was resolved at 500 nl/min using linear gradients from 0% to 45% (v/v) acetonitrile in 0.2% (v/v) formic acid. Proteome Discoverer 1.4 (Thermo Scientific) was used to process the data, and the CCT1 sequence was searched using SEQUEST (Thermo Scientific). Search parameters included a precursor mass tolerance of 10 ppm and a fragment mass tolerance of 0.8 Da. Peptides were searched with carbamidomethyl cysteine as a static modification and oxidized methionine, deamidated glutamine and asparagine, and phosphorylated Ser as dynamic modifications.

Liposome binding assay

The liposome binding assay was carried out as reported previously (17). Two hundred micrograms of PC and PA at different mole ratios were mixed and dried. TBS (pH 7.0, 100 μl) was added to the lipids, and the mixture was incubated at 37 °C for 1 h and vortexed for 5 min. To obtain liposomes, the mixtures were spun at 16,000 $\times$ *g* for 10 min and washed with cold TBS. Purified AtCCT1 (50 μg/ml) was spun at 16,000 $\times$ *g* for 10 min at 4 °C, and 100 μl of the supernatant was added to the precipitated liposomes, followed by incubation at room temperature for 45 min and on ice for 15 min. Liposomes with bound proteins were recovered by centrifugation at 16,000 $\times$ *g* for 10 min at 4 °C and washed twice with ice-cold TBS. To analyze the amount of proteins bound, the mixture was either subjected to SDS-PAGE or Western blotting using anti-HisG-HRP antibody.

Transient expression of target genes in N. benthamiana leaves

N. benthamiana was grown in a growth chamber set at 25 °C, 50% humidity and 16/8 h day/night cycles. *Agrobacterium tumefaciens* GV3101 cells were individually transformed with the p19 vector encoding a viral suppressor protein and pGREEN 0229 vectors with *AtCCT1-CD* and *SnRK1* genes under the *Cam35S* promoter. Different combinations (p19, p19/AtCCT1, and p19/AtCCT1/SnRK1) of the cultures were mixed in transformation medium (50 mM MES, 2 mM Na_3PO_4: $12H_2O$, 0.5% (w/v) glucose, and 0.1 mM acetosyringone) with a final A_{600} of 0.125 for each culture. Fifteen leaves from five

plants (three leaves per plant) were infiltrated with the various gene combinations. Each leaf was injected with all combinations at random positions. After 5 days, leaf discs with similar treatments from the same plants were obtained, pooled, and freeze-dried.

Lipid extraction from N. benthamiana leaves and PC analysis

Total lipids were extracted from lyophilized leaf samples (~70 mg) by homogenizing in chloroform:isopropanol (2:1 (v/v)) as described previously (51). For quantification, 100 μg of 1,2-dinonadecanoyl-*sn*-glycero-3-phosphocholine (C19:0 PC) was added to each sample as a PC internal standard. The extracted lipids were then separated on TLC plates (0.25-mm silica gel, DC-Fertigplatten, Macherey-Nagel, Germany) using acetone:toluene:water (91:30:7.5 (v/v/v)) as the mobile phase (52). PC bands on the TLC plate were visualized under UV light by primulin staining, scraped, and then transmethylated by incubation with 3 N methanolic HCl for 1 h at 80 °C. The resulting fatty acid methyl esters were then analyzed on an Agilent 6890N Gas Chromatograph equipped with a 5975 Inert XL Mass Selective Detector (Agilent Technologies) using a capillary column DB 23 (30 m × 0.25 mm × 0.25 μm, Agilent Technologies, Wilmington, DE). The GC parameters were as follows: 165 °C for 4 min, increased to 180 °C at 10 °C/min and held for 5 min, and increased to 230 °C at 10 °C/min and held for 5 min.

Author contributions—K. M. P. C. and G. C. conceptualization; K. M .P. C., Y. X., and L. F. data curation; K. M. P. C., Y. X., L. F., and G. C. formal analysis; K. M. P. C., Y. X., L. F., and G. C. validation; K. M. P. C., Y. X., L. F., K. J., J. Z. A., and G. C. investigation; K. M. P. C., Y. X., L. F., and G. C. methodology; K. M. P. C., Y. X., L. F., and G. C. writing-original draft; K. M. P. C., Y. X., L. F., K. J., J. Z. A., and G. C. writing-review and editing; J. Z. A. software; G. C. resources; G. C. supervision; G. C. funding acquisition; G. C. project administration.

Acknowledgments—We thank Jack Moore (Alberta Proteomics and Mass Spectrometry Facility) for assistance with LC-MS/MS analysis, Dr. Stacy Singer (Agriculture and Agri-Food Canada) for sharing knowledge regarding tobacco leaf transient expression, Dr. Shanjida Khan (University of Alberta) for providing the N. benthamiana seeds, Dr. Wei Shen (North Carolina State University) for the SnRK1 and GRIK1 expression plasmids, and Dr. Rosemary Cornell (Simon Fraser University) for valuable discussions.

References

1. Ohlrogge, J., and Browse, J. (1995) Lipid biosynthesis. *Plant Cell* **7,** 957–970 CrossRef Medline
2. Gibellini, F., and Smith, T. K. (2010) The Kennedy pathway: *de novo* synthesis of phosphatidylethanolamine and phosphatidylcholine. *IUBMB Life* **62,** 414–428 Medline
3. Kennedy, E. P. (1958) The biosynthesis of phospholipids. *Am. J. Clin. Nutr.* **6,** 216–220 CrossRef Medline
4. Moore, T. S. (1982) Phospholipid biosynthesis. *Annu. Rev. Plant Physiol.* **33,** 235–259 CrossRef
5. Sparace, S. A., and Moore, T. S. (1981) Phospholipid metabolism in plant mitochondria: II: submitochondrial sites of synthesis of phosphatidylcholine and phosphatidylethanolamine. *Plant Physiol.* **67,** 261–265 CrossRef Medline
6. Craddock, C. P., Adams, N., Bryant, F. M., Kurup, S., and Eastmond, P. J. (2015) Phosphatidic acid phosphohydrolase regulates phosphatidylcholine biosynthesis in *Arabidopsis* by phosphatidic acid-mediated activation of CTP:phosphocholine cytidylyltransferase activity. *Plant Cell* **27,** 1251–1264 CrossRef Medline
7. Tasseva, G., Richard, L., and Zachowski, A. (2004) Regulation of phosphatidylcholine biosynthesis under salt stress involves choline kinases in *Arabidopsis thaliana*. *FEBS Lett.* **566,** 115–120 CrossRef Medline
8. Choi, S. B., Lee, K. W., and Cho, S. H. (1997) Cloning of CTP:phosphocholine cytidylyltransferase cDNA from *Arabidopsis thaliana*. *Mol. Cells* **7,** 58–63 Medline
9. Wurzinger, B., Nukarinen, E., Nägele, T., Weckwerth, W., and Teige, M. (2018) The SnRK1 kinase as central mediator of energy signaling between different organelles. *Plant Physiol.* **176,** 1085–1094 CrossRef Medline
10. Halford, N. G., Hey, S., Jhurreea, D., Laurie, S., McKibbin, R. S., Paul, M., and Zhang, Y. (2003) Metabolic signalling and carbon partitioning: role of Snf1-related (SnRK1) protein kinase. *J. Exp. Bot.* **54,** 467–475 CrossRef Medline
11. Sugden, C., Donaghy, P. G., Halford, N. G., and Hardie, D. G. (1999) Two SNF1-related protein kinases from spinach leaf phosphorylate and inactivate 3-hydroxy-3-methylglutaryl-coenzyme A reductase, nitrate reductase, and sucrose phosphate synthase *in vitro*. *Plant Physiol.* **120,** 257–274 CrossRef Medline
12. Tiessen, A., Prescha, K., Branscheid, A., Palacios, N., McKibbin, R., Halford, N. G., and Geigenberger, P. (2003) Evidence that SNF1-related kinase and hexokinase are involved in separate sugar-signalling pathways modulating post-translational redox activation of ADP-glucose pyrophosphorylase in potato tubers. *Plant J.* **35,** 490–500 CrossRef Medline
13. Purcell, P. C., Smith, A. M., and Halford, N. G. (1998) Antisense expression of a sucrose non-fermenting-1-related protein kinase sequence in potato results in decreased expression of sucrose synthase in tubers and loss of sucrose-inducibility of sucrose synthase transcripts in leaves. *Plant J.* **14,** 195–202 CrossRef
14. Laurie, S., McKibbin, R. S., and Halford, N. G. (2003) Antisense SNF1-related (SnRK1) protein kinase gene represses transient activity of an α-amylase (α-Amy2) gene promoter in cultured wheat embryos. *J. Exp. Bot.* **54,** 739–747 CrossRef Medline
15. Zhai, Z., Liu, H., and Shanklin, J. (2017) Phosphorylation of WRINKLED1 by KIN10 results in its proteasomal degradation, providing a link between energy homeostasis and lipid biosynthesis. *Plant Cell* **29,** 871–889 CrossRef Medline
16. Zhai, Z., Keereetaweep, J., Liu, H., Feil, R., Lunn, J. E., and Shanklin, J. (2018) Trehalose 6-phosphate positively regulates fatty acid synthesis by stabilizing WRINKLED1. *Plant Cell* **30,** 2616–2627 CrossRef Medline
17. Caldo, K. M. P., Shen, W., Xu, Y., Hanley-Bowdoin, L., Chen, G., Weselake, R. J., and Lemieux, M. J. (2018) Diacylglycerol acyltransferase 1 is activated by phosphatidate and inhibited by SnRK1-catalyzed phosphorylation. *Plant J.* **96,** 287–299 CrossRef Medline
18. Xu, Y., Caldo, K. M. P., Pal-Nath, D., Ozga, J., Lemieux, M. J., Weselake, R. J., and Chen, G. (2018) Properties and biotechnological applications of acyl-CoA:diacylglycerol acyltransferase and phospholipid:diacylglycerol acyltransferase from terrestrial plants and microalgae. *Lipids* **53,** 663–688 CrossRef Medline
19. Caldo, K. M. P., Acedo, J. Z., Panigrahi, R., Vederas, J. C., Weselake, R. J., and Lemieux, M. J. (2017) Diacylglycerol acyltransferase 1 is regulated by its N-terminal domain in response to allosteric effectors. *Plant Physiol.* **175,** 667–680 Medline
20. Cornell, R. B., Kalmar, G. B., Kay, R. J., Johnson, M. A., Sanghera, J. S., and Pelech, S. L. (1995) Functions of the C-terminal domain of CTP:phosphocholine cytidylyltransferase: effects of C-terminal deletions on enzyme activity, intracellular localization and phosphorylation potential. *Biochem. J.* **310,** 699–708 CrossRef Medline
21. Cornell, R. B., and Northwood, I. C. (2000) Regulation of CTP:phosphocholine cytidylyltransferase by amphitropism and relocalization. *Trends Biochem. Sci.* **25,** 441–447 CrossRef Medline
22. Brault, J. P., and Friesen, J. A. (2016) Characterization of cytidylyltransferase enzyme activity through high performance liquid chromatography. *Anal. Biochem.* **510,** 26–32 CrossRef Medline

23. Arnold, R. S., and Cornell, R. B. (1996) Lipid regulation of CTP: phosphocholine cytidylyltransferase: electrostatic, hydrophobic, and synergistic interactions of anionic phospholipids and diacylglycerol. *Biochemistry* **35,** 9917–9924 CrossRef Medline
24. Ding, Z., Taneva, S. G., Huang, H. K., Campbell, S. A., Semenec, L., Chen, N., and Cornell, R. B. (2012) A 22-mer segment in the structurally pliable regulatory domain of metazoan CTP:phosphocholine cytidylyltransferase facilitates both silencing and activating functions. *J. Biol. Chem.* **287,** 38980–38991 CrossRef Medline
25. Lee, J., Taneva, S. G., Holland, B. W., Tieleman, D. P., and Cornell, R. B. (2014) Structural basis for autoinhibition of CTP:phosphocholine cytidylyltransferase (CCT), the regulatory enzyme in phosphatidylcholine synthesis, by its membrane-binding amphipathic helix. *J. Biol. Chem.* **289,** 1742–1755 CrossRef Medline
26. Cornell, R. (1989) Chemical cross-linking reveals a dimeric structure for CTP:phosphocholine cytidylyltransferase. *J. Biol. Chem.* **264,** 9077–9082 Medline
27. Rao, S. T., and Rossmann, M. G. (1973) Comparison of super-secondary structures in proteins. *J. Mol. Biol.* **76,** 241–256 CrossRef Medline
28. Helmink, B. A., Braker, J. D., Kent, C., and Friesen, J. A. (2003) Identification of lysine 122 and arginine 196 as important functional residues of rat CTP:phosphocholine cytidylyltransferase alpha. *Biochemistry* **42,** 5043–5051 CrossRef Medline
29. Ramezanpour, M., Lee, J., Taneva, S. G., Tieleman, D. P., and Cornell, R. B. (2018) An auto-inhibitory helix in CTP:phosphocholine cytidylyltransferase hijacks the catalytic residue and constrains a pliable, domain-bridging helix pair. *J. Biol. Chem.* **293,** 7070–7084 CrossRef Medline
30. Ward, J. J., Sodhi, J. S., McGuffin, L. J., Buxton B. F., and Jones, D. T. (2004) Prediction and functional analysis of native disorder in proteins from the three kingdoms of life. *J. Mol. Biol.* **337,** 635–645 CrossRef Medline
31. Wang, Y., MacDonald, J. I., and Kent, C. (1995) Identification of the nuclear localization signal of rat liver CTP:phosphocholine cytidylyltransferase. *J. Biol. Chem.* **270,** 354–360 CrossRef Medline
32. Hornbeck, P. V., Zhang, B., Murray, B., Kornhauser, J. M., Latham, V., and Skrzypek, E. (2015) PhosphoSitePlus, 2014: mutations, PTMs and recalibrations. *Nucleic Acids Res.* **43,** D512–20 CrossRef Medline
33. Durek, P., Schmidt, R., Heazlewood, J. L., Jones, A., MacLean, D., Nagel, A., Kersten, B., and Schulze, W. X. (2010) PhosPhAt: the *Arabidopsis thaliana* phosphorylation site database: an update. *Nucleic Acids Res.* **38,** D828–34 CrossRef Medline
34. Wang, X., Bian, Y., Cheng, K., Gu, L. F., Ye, M., Zou, H., Sun, S. S., and He, J. X. (2013) A large-scale protein phosphorylation analysis reveals novel phosphorylation motifs and phosphoregulatory networks in *Arabidopsis*. *J. Proteomics* **78,** 486–498 CrossRef Medline
35. Roitinger, E., Hofer, M., Köcher, T., Pichler, P., Novatchkova, M., Yang, J., Schlögelhofer, P., and Mechtler, K. (2015) Quantitative phosphoproteomics of the ataxia telangiectasia-mutated (ATM) and ataxia telangiectasia-mutated and rad3-related (ATR) dependent DNA damage response in *Arabidopsis thaliana*. *Mol. Cell. Proteomics* **14,** 556–571 CrossRef Medline
36. Shen, W., Reyes, M. I., and Hanley-Bowdoin, L. (2009) *Arabidopsis* protein kinases GRIK1 and GRIK2 specifically activate SnRK1 by phosphorylating its activation loop. *Plant Physiol.* **150,** 996–1005 CrossRef Medline
37. Hatch, G. M., Jamil, H., Utal, A. K., and Vance, D. E. (1992) On the mechanism of the okadaic acid-induced inhibition of phosphatidylcholine biosynthesis in isolated rat hepatocytes. *J. Biol. Chem.* **267,** 15751–15758 Medline
38. Veitch, D. P., Gilham, D., and Cornell, R. B. (1998) The role of histidine residues in the HXGH site of CTP:phosphocholine cytidylyltransferase in CTP binding and catalysis. *Eur. J. Biochem.* **255,** 227–234 CrossRef Medline
39. Cornell, R. B. (2016) Membrane lipid compositional sensing by the inducible amphipathic helix of CCT. *Biochim. Biophys. Acta* **1861,** 847–861 CrossRef Medline
40. Pelech, S. L., and Vance, D. E. (1989) Signal transduction via phosphatidylcholine cycles. *Trends Biochem. Sci.* **14,** 28–30 CrossRef
41. Tronchère, H., Record, M., Tercé, F., and Chap, H. (1994) Phosphatidylcholine cycle and regulation of phosphatidylcholine biosynthesis by enzyme translocation. *Biochim. Biophys. Acta* **1212,** 137–151 CrossRef Medline
42. Brown, C. J., Takayama, S., Campen, A. M., Vise, P., Marshall, T. W., Oldfield, C. J., Williams, C. J., and Dunker, A. K. (2002) Evolutionary rate heterogeneity in proteins with long disordered regions. *J. Mol. Evol.* **55,** 104–110 CrossRef Medline
43. Wright, P. E., and Dyson, H. J. (2015) Intrinsically disordered proteins in cellular signalling and regulation. *Nat. Rev. Mol. Cell Biol.* **16,** 18–29 CrossRef Medline
44. Dale, S., Arró, M., Becerra, B., Morrice, N. G., Boronat, A., Hardie, D. G., and Ferrer, A. (1995) Bacterial expression of the catalytic domain of 3-hydroxy-3-methylglutaryl-CoA reductase (isoform HMGR1) from *Arabidopsis thaliana*, and its inactivation by phosphorylation at Ser577 by *Brassica oleracea* 3-hydroxy-3-methylglutaryl-CoA reductase kinase. *Eur. J. Biochem.* **233,** 506–513 CrossRef Medline
45. Bachmann, M., Shiraishi, N., Campbell, W. H., Yoo, B. C., Harmon, A. C., and Huber, S. C. (1996) Identification of Ser-543 as the major regulatory phosphorylation site in spinach leaf nitrate reductase. *Plant Cell* **8,** 505–517 CrossRef Medline
46. Huang, A. H. C. (2018) Plant lipid droplets and their associated proteins: potential for rapid advances. *Plant Physiol.* **176,** 1894–1918 CrossRef Medline
47. Toroser, D., Plaut, Z., and Huber, S. C. (2000) Regulation of a plant SNF1-related protein kinase by glucose-6-phosphate. *Plant Physiol.* **123,** 403–412 CrossRef Medline
48. Zhang, Y., Primavesi, L. F., Jhurreea, D., Andralojc, P. J., Mitchell, R. A., Powers, S. J., Schluepmann, H., Delatte, T., Wingler, A., and Paul, M. J. (2009) Inhibition of SNF1-related protein kinase1 activity and regulation of metabolic pathways by trehalose-6-phosphate. *Plant Physiol.* **149,** 1860–1871 CrossRef Medline
49. Nunes, C., Primavesi, L. F., Patel, M. K., Martinez-Barajas, E., Powers, S. J., Sagar, R., Fevereiro, P. S., Davis, B. G., and Paul, M. J. (2013) Inhibition of SnRK1 by metabolites: tissue-dependent effects and cooperative inhibition by glucose 1-phosphate in combination with trehalose 6-phosphate. *Plant Physiol. Biochem.* **63,** 89–98 CrossRef Medline
50. Buchan, D. W., Minneci, F., Nugent, T. C., Bryson, K., and Jones, D. T. (2013) Scalable web services for the PSIPRED protein analysis workbench. *Nucleic Acids Res.* **41,** W349–W57 CrossRef Medline
51. Mietkiewska, E., Miles, R., Wickramarathna, A., Sahibollah, A. F., Greer, M. S., Chen, G., and Weselake, R. J. (2014) Combined transgenic expression of *Punica granatum* conjugase (FADX) and FAD2 desaturase in high linoleic acid *Arabidopsis thaliana* mutant leads to increased accumulation of punicic acid. *Planta* **240,** 575–583 CrossRef Medline
52. Wang, Z., and Benning, C. (2011) *Arabidopsis thaliana* polar glycerolipid profiling by thin layer chromatography (TLC) coupled with gas-liquid chromatography (GLC). *J. Vis. Exp.* **49,** 2518 CrossRef Medline